

SUPPORTING INFORMATION

Supporting Information

Photocatalytic Generation of a Non-Heme Fe(III)-Hydroperoxo Species with O₂ in Water for Oxygen Atom Transfer Reaction

Eva Pugliese,^[a] Nhat Tam Vo,^[a] Alain Boussac,^[b] Frédéric Banse,^[a] Yasmina Mekmouche,^[c] Jalila Simaan,^[c] Thierry Tron,^[c] Philipp Gotico,^[b] Marie Sircoglou,^[a] Zakaria Halime,^[a] Winfried Leibl*^[b] and Ally Aukauloo*^[a, b]

Abstract: Using only light energy and dioxygen (O₂) to drive oxygenation reactions is an interesting strategy to avoid the use of hazardous oxidizing agents. Coupling a photoredox module and a bio-inspired non-heme model to activate O₂ for oxygen atom transfer (OAT) reaction requires a vigorous investigation to shed light on the multiple competing electron transfer steps, charge accumulation and annihilation processes, and the activation of O₂ at the catalytic unit. We found that the efficient oxidative quenching mechanism between [Ru(bpy)₃]²⁺ chromophore and a reversible electron mediator, methyl viologen (MV²⁺), to form the reducing species methyl viologen radical (MV^{•+}) can convey an electron to O₂ to form the superoxide radical and resetting an Fe(III) species in a catalytic cycle to the Fe(II) state in an aqueous solution. The reaction between these two one-electron reduced species under pH control leads to the formation of the Fe(III)-hydroperoxo (Fe^{III}-OOH) intermediate that ultimately can evolve to highly oxidized iron-oxo species to perform the OAT reaction to an alkene substrate. Such a strategy allows to bypass the challenging task of charge accumulation at the molecular catalytic unit for the two-electron activation of O₂. The Fe^{III}-OOH catalytic precursor was trapped and characterized by EPR spectroscopy pertaining a metal assisted catalysis. Laser Flash Photolysis (LFP) studies and spectroscopic monitoring during photocatalysis lend credence to the proposed catalytic cycle.

DOI: 10.1002/anie.2021XXXXX

SUPPORTING INFORMATION

Table of Contents

Experimental Procedures	3
Materials and Instrumentation	3
Synthesis	3
Kinetic analysis	3
Laser flash photolysis	4
Figure S1	4
Figure S2	4
Figure S3	5
Figure S4	5
Figure S5	6
Cyclic voltammetry	6
Figure S6	6
Photocatalysis	7
Table S1	7
Figure S7	8
Figure S8	8
Isotope labelling study	9
Figure S9	9
Figure S10	9
UV-visible absorption spectra	10
Figure S11	10
Figure S12	10
Figure S13	11
Electronic paramagnetic resonance spectra	12
Figure S14	12
Figure S15	13
Figure S16	13
Figure S17	13
Cis-diol and aldehyde formation from iron hydro(peroxo) species	14
Scheme S1	14
References	14

SUPPORTING INFORMATION

Experimental Procedures

Materials and Instrumentation

Iron (II) triflate, methyl viologen dichloride hydrate (98 %) and sodium 4-styrenesulfonate were purchased from Sigma-Aldrich. Deuterium oxide and dioxygen- ^{18}O (97 %) were purchased from EURISO-TOP.

UV-visible absorption spectra were recorded in solution using 1 cm quartz cuvettes on a Varian Cary 60 UV-vis spectrophotometer. NMR spectroscopic measurements were performed using a Bruker Avance III 400 MHz. Photocatalysis experiments were carried out in Britton & Robinson (B&R) buffer pH 4.0 at 25 °C with a white LED from Metaphase Technology equipped with a Wratten 2B filter $\lambda > 450$ nm. The high performance liquid chromatography experiments (HPLC) were performed on 1260 infinity II LC system (Zorbax Eclipse Plus C18 column) from Agilent Technologies. The Thermo Scientific DSQ 2004 model from Thermo Fischer Scientific Company was employed for recording the electrospray ionization mass spectrometry experiments with an ESI⁻ method.

Photocatalysis experiments under $^{18}\text{O}_2$ atmosphere were prepared in a Schlenk tube. The reaction mixture was subjected to 3 times vacuum/argon cycles then one time vacuum/ $^{18}\text{O}_2$. After reaction, samples were treated with 1M HCl then extracted with ethyl acetate. The products formed were separated by preparative HPLC then analyzed by HRMS-ESI⁻. Their identification and quantification was achieved by ^1H NMR with addition of 10% deuterium oxide to be used as reference. The substrate and products were identified and quantified from the following peaks: styrene sulfonate by doublet at 6.75 ppm, benzaldehyde by singlet at 9.91 ppm, diol by doublet at 7.42 ppm, epoxide by doublet at 7.37 ppm.

For Laser Flash Photolysis (LFP) experiments, samples were prepared in 1 cm quartz cuvettes. Transient absorption and emission measurements were recorded on an Edinburgh Instruments LP920 laser flash photolysis spectrometer. Laser excitation pulses were generated from a Continuum Surelite OPO laser (5 ns pulses duration, typical energy 10 mJ per flash) for excitation at 460 nm. The probe source is a pulsed 450 W Xenon lamp and the detectors are either a Hamamatsu photomultiplier tube (PMT) or a water-cooled Andor intensified charge coupled device (ICCD) camera.

For Electron Paramagnetic Resonance (EPR) measurement, X-band cw-EPR spectra were recorded with a Bruker Elexsys 500 X-band spectrometer equipped with a standard ER 4102 (Bruker) X-band resonator, a Bruker teslameter, an Oxford Instruments cryostat (ESR 900) and an Oxford ITC504 temperature controller.

Synthesis

$[(\text{L}_5)\text{Fe}^{\text{II}}]^{2+}$ was synthesized in a glovebox. $\text{Fe}(\text{OTf})_2 \cdot 2 \text{ MeCN}$ (475 mg, 1.09 mmol, 1 eq.) was suspended in MeOH/MeCN 4/1 (5 mL) and added dropwise to a solution of the ligand L_5 (389 mg, 1.12 mmol, 1 eq.) dissolved in 3 mL MeOH. The brown solution immediately obtained was stirred for 2 hours after which diethyl ether (30 mL) was added to yield an ochre precipitate. The solid was isolated by filtration, washed with Et_2O (3 \times 5 mL) and finally dried under vacuum. ESI⁺-HRMS: calculation for $[\text{C}_{21}\text{H}_{25}\text{N}_5\text{Fe}]^{2+}$ 201.5725; found 201.5667; UV-vis (H_2O): 390 nm ($t_{2g}(\text{Fe}^{\text{II}})$ -to- $\pi^*(\text{py})$) $\epsilon = 6000 \text{ M}^{-1}\cdot\text{cm}^{-1}$; UV-vis (acetone): 392 nm ($t_{2g}(\text{Fe}^{\text{II}})$ -to- $\pi^*(\text{py})$) $\epsilon = 1500 \text{ M}^{-1}\cdot\text{cm}^{-1}$; UV-vis (MeOH): 394 nm ($t_{2g}(\text{Fe}^{\text{II}})$ -to- $\pi^*(\text{py})$) $\epsilon = 2000 \text{ M}^{-1}\cdot\text{cm}^{-1}$; UV-vis (MeCN): 390 nm ($t_{2g}(\text{Fe}^{\text{II}})$ -to- $\pi^*(\text{py})$) $\epsilon = 5000 \text{ M}^{-1}\cdot\text{cm}^{-1}$. All of these features conform to published data.¹⁻⁴

Kinetic analysis

Analysis of transient absorption data (Fig. S2, S3) was performed using the KinTek Explorer simulation Program.^{5,6}

SUPPORTING INFORMATION

Laser flash photolysis

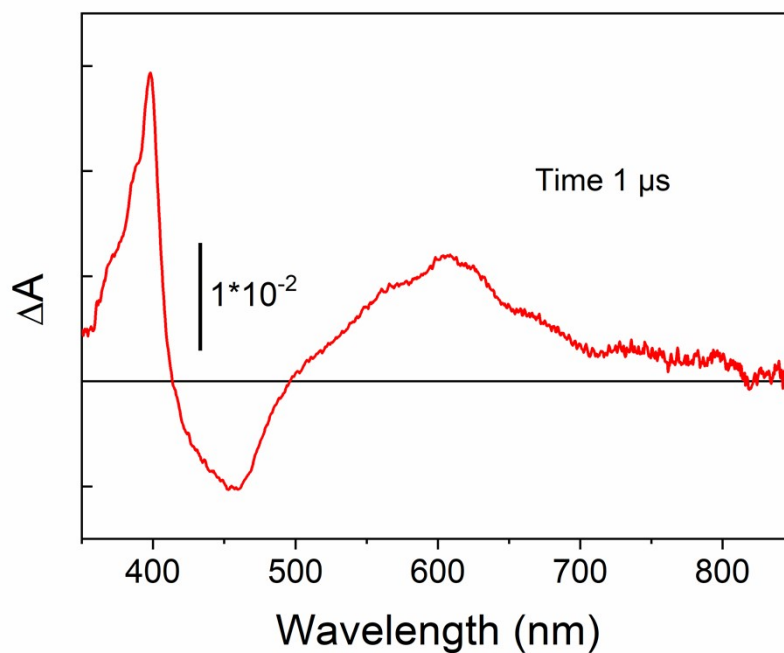


Figure S1 Transient absorption spectrum from a B&R pH 4 buffer solution of $[\text{Ru}^{\text{II}}(\text{bpy})_3]\text{Cl}_2$ (30 μM), MV^{2+} (4 mM) in air at 1 μs delay after excitation.

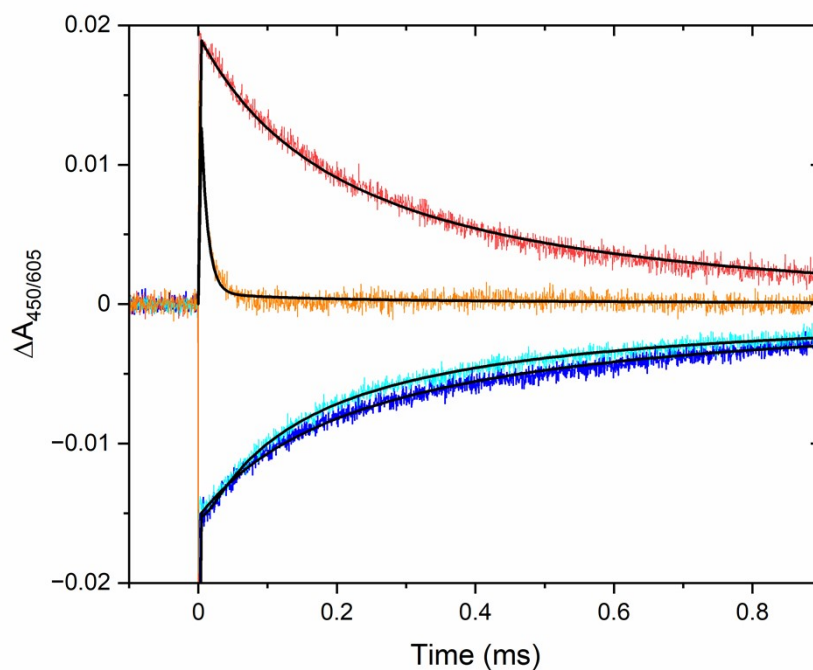


Figure S2 Time-resolved absorption changes of a solution of $[\text{Ru}^{\text{II}}(\text{bpy})_3]\text{Cl}_2$ (30 μM) and MV^{2+} (4 mM) at 450 nm (blue) and 605 nm (red) in argon saturated B&R pH 4 buffer; at 450 nm (cyan) and 605 nm (orange) in B&R pH 4 buffer under aerobic conditions. Solid black lines are best fit traces

SUPPORTING INFORMATION

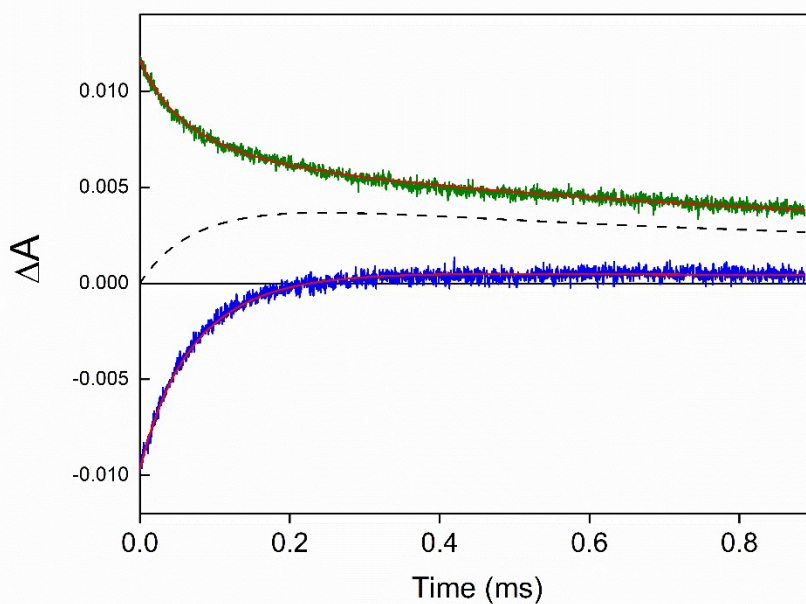


Figure S3 Time-resolved absorption changes of a solution of $[\text{Ru}^{\text{II}}(\text{bpy})_3]\text{Cl}_2$ (30 μM) and MV^{2+} (4 mM) at 450 nm (blue) and 605 nm (green) in Ar-saturated B&R buffer (pH 4) in presence of sodium 4-styrenesulfonate (100 mM). Red traces: kinetic analysis yielding second order rate constants for charge recombination between $[\text{Ru}^{\text{III}}]$ and MV^{2+} ($9.5 \times 10^9 \text{ M}^{-1}\text{s}^{-1}$; this rate is increased by about a factor of 2 attributed to the very high concentration of styrene in this particular experiment), sodium 4-styrenesulfonate oxidation by $[\text{Ru}^{\text{III}}]$ ($7.3 \times 10^4 \text{ M}^{-1}\text{s}^{-1}$) and charge recombination between MV^{2+} and oxidized sodium 4-styrenesulfonate ($1.9 \times 10^9 \text{ M}^{-1}\text{s}^{-1}$). The dashed line indicates the concentration of oxidized styrene, with the maximum corresponding to a concentration of 0.4 μM . Initial concentration of Ru(III) and MV^{2+} : 0.85 μM .

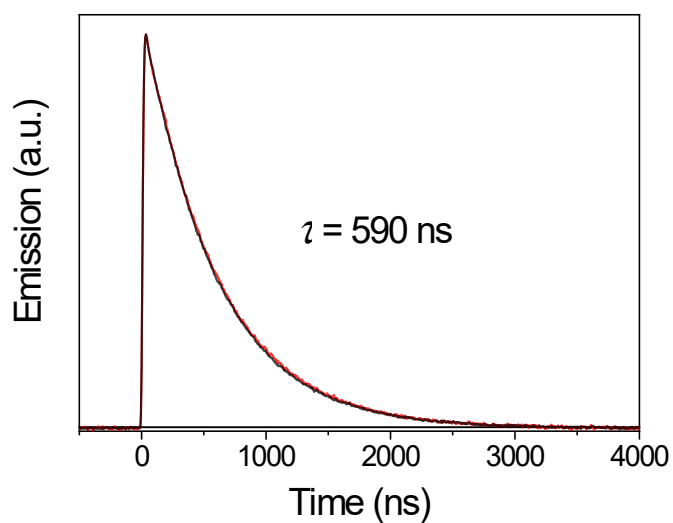


Figure S4 Normalized traces of the kinetics of $[\text{Ru}^{\text{II}}]^*$ emission measured at 610 nm in a B&R pH 4 solution of $[\text{Ru}^{\text{II}}(\text{bpy})_3]\text{Cl}_2$ (30 μM) (red) in the absence and (black) presence of $[(\text{L}_5)\text{Fe}^{\text{II}}]^{2+}$ (30 μM).

SUPPORTING INFORMATION

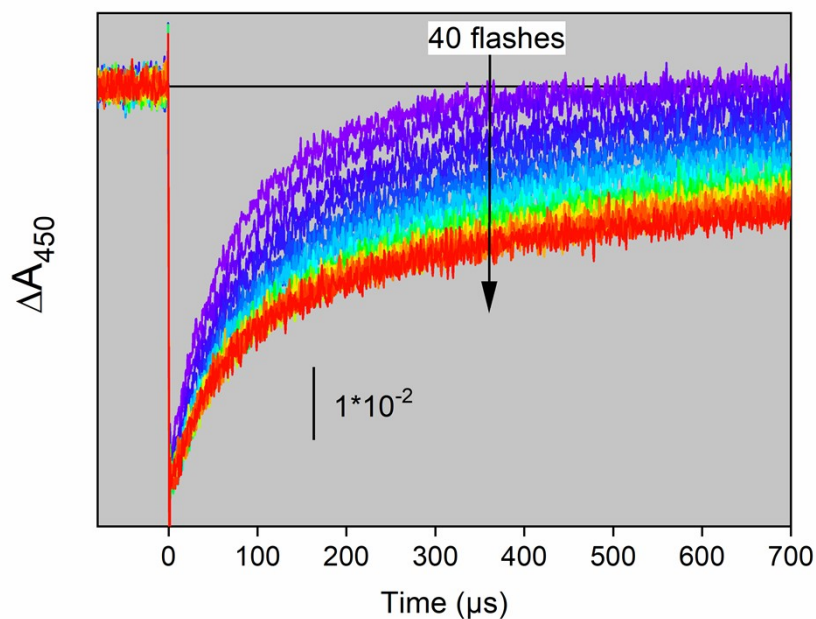


Figure S5 Time-resolved absorption changes at 450 nm of a solution of $[\text{Ru}^{\text{II}}(\text{bpy})_3]\text{Cl}_2$ (30 μM), MV^{2+} (20 mM), $[(\text{L}_5)\text{Fe}^{\text{II}}]^{2+}$ (100 μM) in B&R pH 4 buffer under aerobic conditions. Each trace is an average of two flashes showing progressive transition from fast (violet) to slow (red) Ru(III) recovery kinetics. Related to Fig. 1B of the main paper.

Cyclic voltammetry

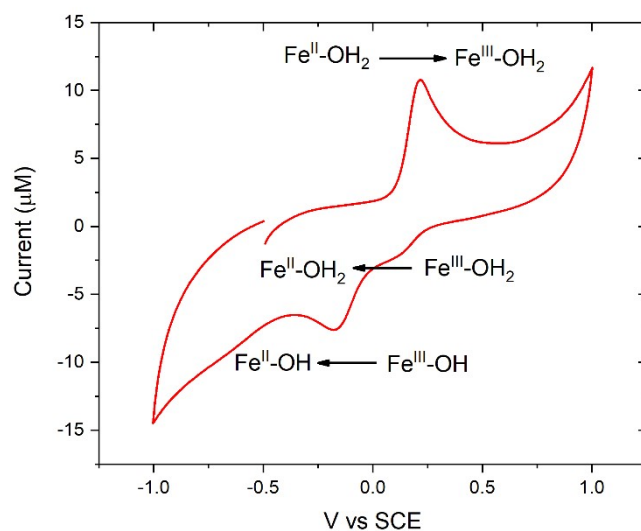


Figure S6 Cyclic voltammetry of 1 mM $[(\text{L}_5)\text{Fe}^{\text{II}}]^{2+}$ at 0.1 V/s in an aqueous medium buffered at pH 6. Supporting electrolyte: 0.1 M NaClO_4 , working electrode: glassy carbon. The redox couples were attributed to the presence of a water molecule in the coordination sphere of the iron center. The loss in reversibility of the electrochemical oxidation wave was attributed to a proton coupled electron transfer process.

SUPPORTING INFORMATION

Photocatalysis

Table S1 Substrate conversion under different conditions. Oxygenation reactions were carried out under irradiation for 22 hours (backlight white LED = 1.3 mW.cm⁻² equipped with a Wratten filter 2E, $\lambda > 450$ nm), under aerobic conditions, in B&R buffer.

Entry	pH buffer	[Ru ^{II} (bpy) ₃]Cl ₂	[(L ₅)Fe ^{II}] ²⁺	MV ²⁺	Substrate	Product (mM)			TON ^[a]	TOF (h ⁻¹)	φ (%)
						Diol	Benzaldehyde	Epoxide			
1	4	30 μ M	0	0	10 mM	0	0	0	0	0	-
2	4	30 μ M	0	4 mM	10 mM	0	traces	0	nd	nd	-
3	4	0	30 μ M	4 mM	10 mM	0	0	0	0	0	-
4	4	30 μ M	30 μ M	0	10 mM	0	0	0	0	0	-
5	4	30 μ M	30 μ M	4 mM	10 mM	0.83	1.27	traces	70	3.2	2.0
6	4	30 μ M	60 μ M ^[b]	4 mM	10 mM	0	traces	0	nd	nd	-
7	6	30 μ M	30 μ M	4 mM	10 mM	traces	1.17	0.66	61	2.7	1.7

[a] TON: turnover number is calculated over catalyst [b] FeCl₃ is used as catalyst instead of the [(L₅)Fe^{II}]²⁺ complex.

Estimation of Quantum Yield:

The quantum yield for formation of the oxidized products was estimated as follows. The light intensity emitted by the LED panel was measured with a solar power meter as 1.3 mW/cm² and the spectral distribution of the emitted light was measured with an Avantes optical fiber spectrometer showing two bands centered around 450 nm and 560 nm with 30% of the light intensity contained in the 400-500 nm region. The fraction of light absorbed by the [Ru^{II}(bpy)₃]²⁺ chromophore was estimated from the drop of intensity integrated over the 400-500 nm region of the light transmitted through the sample. The number of absorbed photons is $N_{ph} = 5.5 \times 10^{14} \text{ s}^{-1}$ or 4.3×10^{19} for 22 h as used in the photocatalysis experiments.

At pH 4 (entry 5):

The number of product molecules in the 0.5 mL sample is $N_{diol} = 0.83 \text{ mM} \times 0.5 \text{ mL} \times N_{Avo} = 2.5 \times 10^{17}$ and $N_{aldehyde} = 1.27 \text{ mM} \times 0.5 \text{ mL} \times N_{Avo} = 3.8 \times 10^{17}$. Taking into account the number of photons necessary per catalytic cycle (1 for the aldehyde, 2 for the diol) results in an overall quantum yield of $\varphi = [(2 \times N_{diol} + N_{aldehyde}) / N_{ph}] = 2.0\%$.

At pH 6 (entry 7):

The number of product molecules in the 0.5 mL sample is $N_{epoxide} = 0.66 \text{ mM} \times 0.5 \text{ mL} \times N_{Avo} = 4.0 \times 10^{17}$ and $N_{aldehyde} = 1.17 \text{ mM} \times 0.5 \text{ mL} \times N_{Avo} = 3.5 \times 10^{17}$. Taking into account the number of photons necessary per catalytic cycle (1 for the aldehyde, 2 for the epoxide) results in an overall quantum yield of $\varphi = [(2 \times N_{diol} + N_{aldehyde}) / N_{ph}] = 1.7\%$.

SUPPORTING INFORMATION

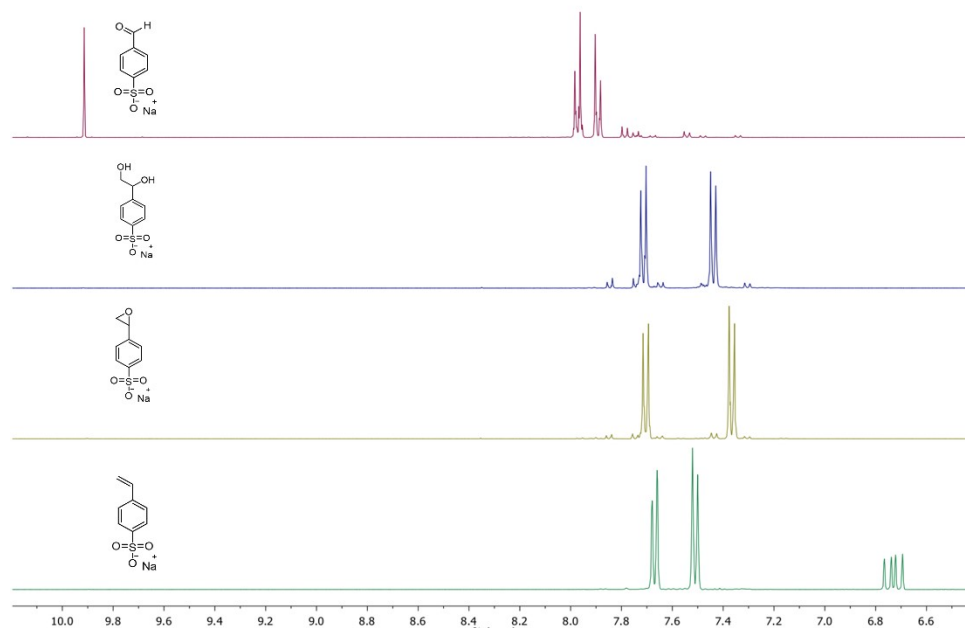
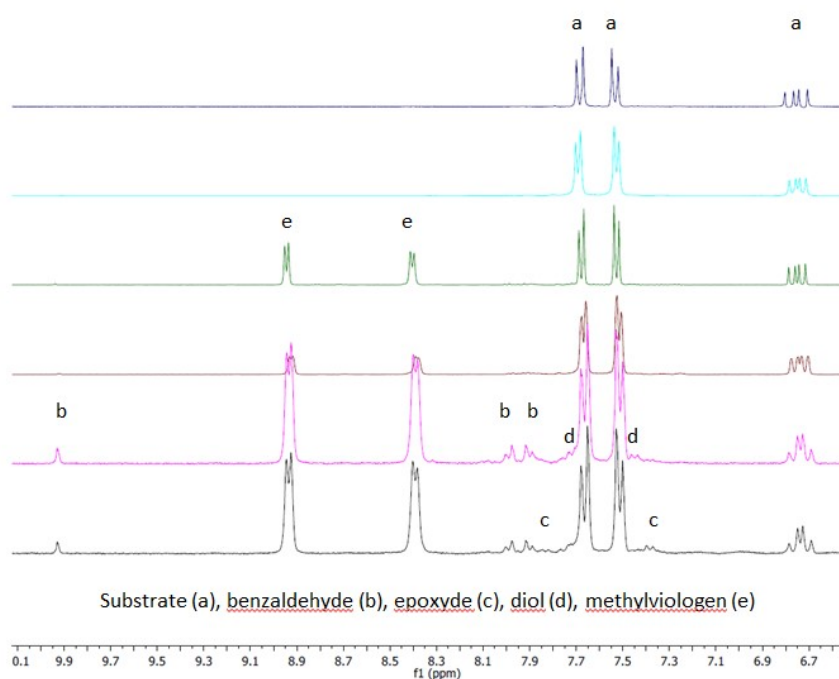


Figure S7 Extracts of the $^1\text{H-NMR}$ spectra of 4-styrenesulfonate, 4-(1,2-dihydroxyethyl)benzenesulfonate, 4-(oxiranyl)benzenesulfonate, 4-formylbenzenesulfonate. Solvent: D_2O



Substrate (a), benzaldehyde (b), epoxyde (c), diol (d), methylviologen (e)

Figure S8 Extracts of the $^1\text{H-NMR}$ spectra of crude reaction mixtures in H_2O and 10% D_2O obtained upon light irradiation of sodium 4-styrenesulfonate (10 mM) for 22 hours under aerobic conditions. (Blue) with $[\text{Ru}^{\text{II}}(\text{bpy})_3]\text{Cl}_2$ (30 μM) in B&R pH 4; (Cyan) with $[\text{Ru}^{\text{II}}(\text{bpy})_3]\text{Cl}_2$ (30 μM) and $[(\text{L}_5)\text{Fe}^{\text{II}}]^{2+}$ (30 μM) in B&R pH 4; (Green) with $[\text{Ru}^{\text{II}}(\text{bpy})_3]\text{Cl}_2$ (30 μM) and MV^{2+} (4 mM) in B&R pH 4; (Brown) with $[\text{Ru}^{\text{II}}(\text{bpy})_3]\text{Cl}_2$ (30 μM), FeCl_3 (60 μM), MV^{2+} (4 mM) in B&R pH 4; (Pink) with $[\text{Ru}^{\text{II}}(\text{bpy})_3]\text{Cl}_2$ (30 μM), $[(\text{L}_5)\text{Fe}^{\text{II}}]^{2+}$ (30 μM), MV^{2+} (4 mM) in B&R pH 4; (Black) with $[\text{Ru}^{\text{II}}(\text{bpy})_3]\text{Cl}_2$ (30 μM), $[(\text{L}_5)\text{Fe}^{\text{II}}]^{2+}$ (30 μM), MV^{2+} (4 mM) in B&R pH 6.

SUPPORTING INFORMATION

Isotope labelling study

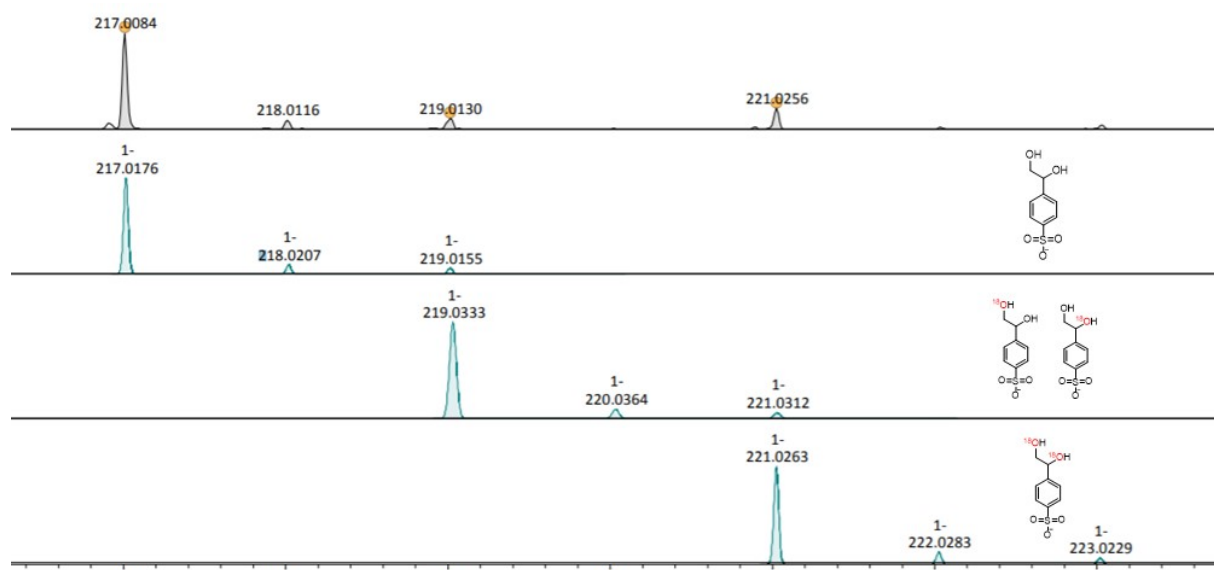


Figure S9 (Black) HRMS-ESI of diol formed in sodium 4-styrenesulfonate oxygenation under irradiation for 22 hours (area backlight white LED = 1 mW.cm⁻² equipped with a Wratten filter 2E, $\lambda > 450$ nm) in B&R pH 4 buffer in presence of [Ru^{II}(bpy)₃]Cl₂ (30 μ M), MV²⁺ (4 mM), [(L₅)Fe^{II}]²⁺ (30 μ M) and sodium 4-styrenesulfonate (10 mM) with ¹⁸O₂ and (Cyan) HRMS-ESI simulations of diol with ¹⁶O and ¹⁸O content.

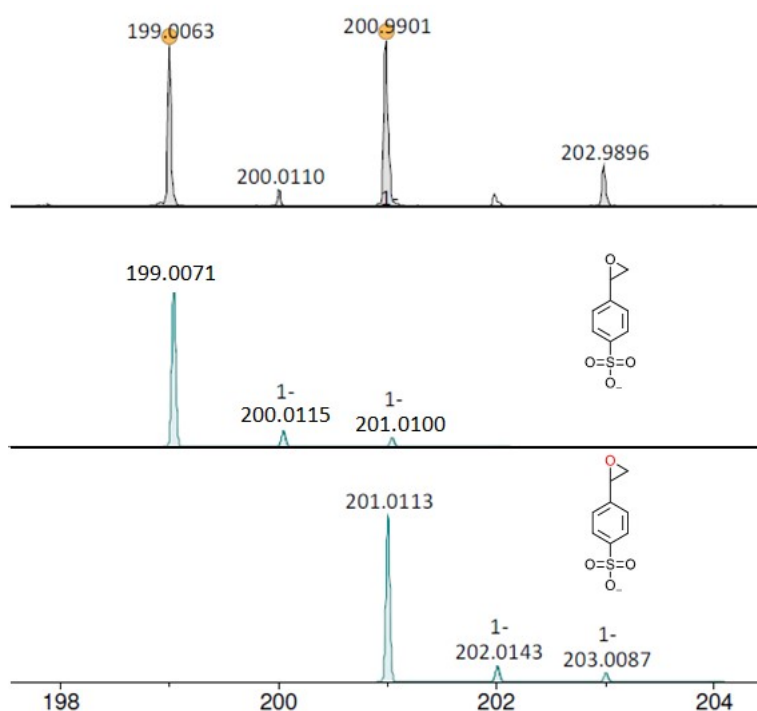


Figure S10 (Black) HRMS-ESI of epoxide formed in sodium 4-styrenesulfonate oxygenation under irradiation for 22 hours (area backlight white LED = 1 mW.cm⁻² equipped with a Wratten filter 2E, $\lambda > 450$ nm) in B&R pH 6 buffer in presence of [Ru^{II}(bpy)₃]Cl₂ (30 μ M), MV²⁺ (4 mM), [(L₅)Fe^{II}]²⁺ (30 μ M) and sodium 4-styrenesulfonate (10 mM) with ¹⁸O₂ and (Cyan) HRMS-ESI simulations of diol with ¹⁶O and ¹⁸O content.

SUPPORTING INFORMATION

UV-visible absorption spectra

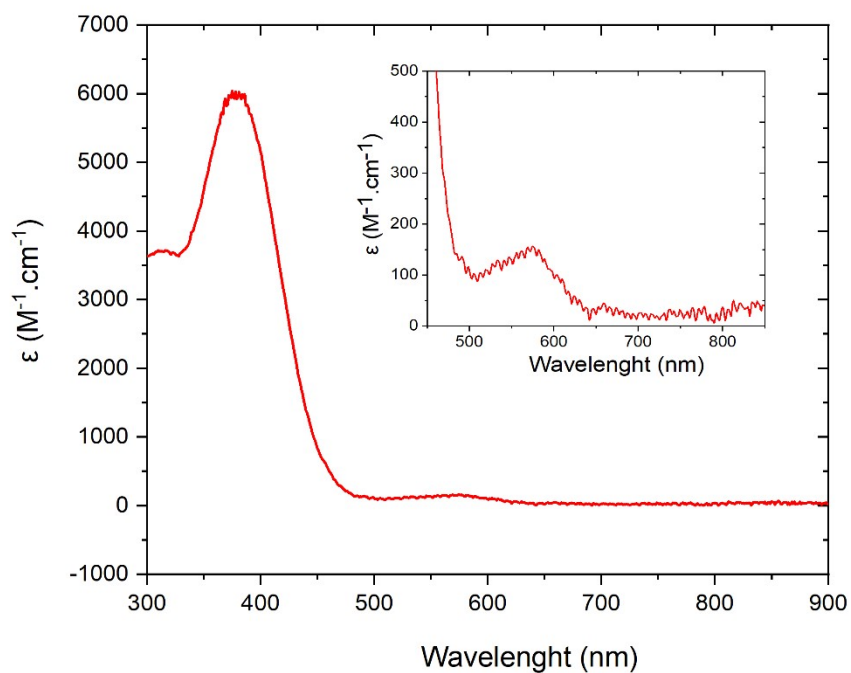


Figure S11 UV-visible spectrum of $[(L_5)Fe^{II}]^{2+}$ complex in B&R pH 4 buffer. Inset: zoom of the 500 - 800 nm window.

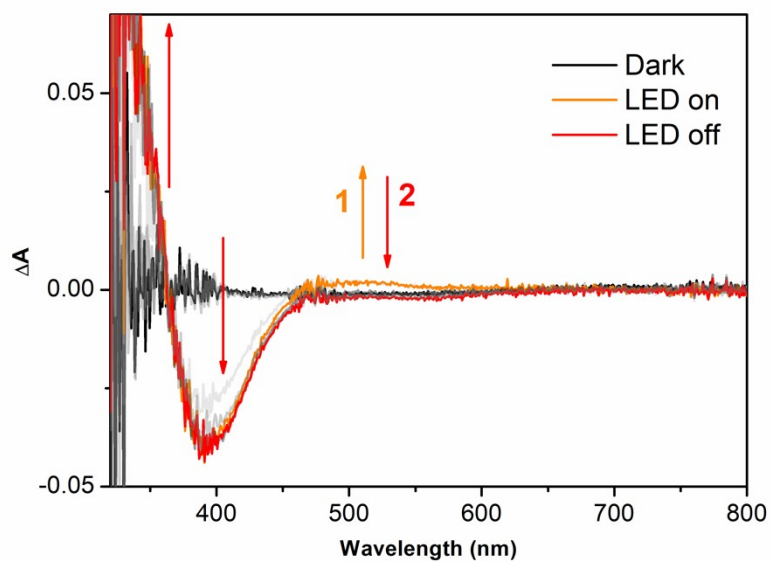


Figure S12 Photoaccumulation of $100 \mu\text{M} [(L_5)Fe^{II}]^{2+}$ in pH 4 buffer in presence of $30 \mu\text{M} [Ru^{II}(bpy)_3]Cl_2$, $10 \text{ mM } MV^{2+}$ and 100 mM styrene sulfonate, at room temperature under aerobic conditions, blue LED, 100 W m^{-2} for 5 s, no stirring.

SUPPORTING INFORMATION

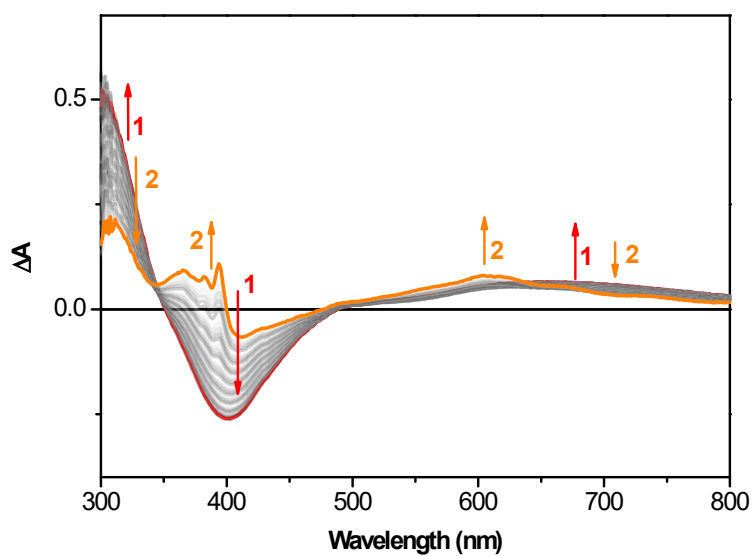


Figure S13 Photoaccumulation of 250 μM $[(L_5)\text{Fe}^{\text{II}}]^{2+}$ in pH 4 buffer in presence of 30 μM $[\text{Ru}^{\text{II}}(\text{bpy})_3]\text{Cl}_2$, 4 mM MV^{2+} and 200 mM TEOA at 5°C under aerobic conditions, blue LED, 100 W m^{-2} continuous light.

SUPPORTING INFORMATION

Electronic paramagnetic resonance spectra

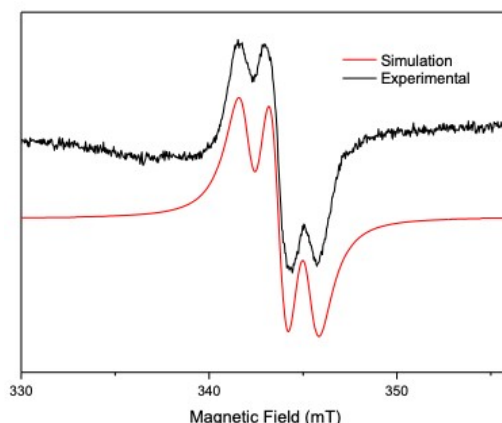
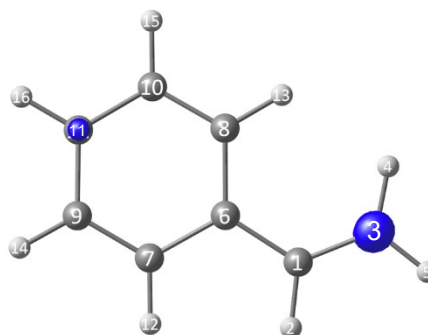


Figure S14 Black : Experimental EPR spectrum of sodium 4-styrenesulfonate radical observed by mixing $[\text{Ru}^{\text{II}}(\text{bpy})_3]^{3+}$ (1 mM) with sodium 4-styrenesulfonate (10 mM) in B&R pH 4 buffer under argon. The spectrum was recorded on a X-band spectrometer at 80 K. Red: Simulated spectrum obtained with a g value of 2.0023, a hyperfine coupling with 2 $S=1/2$ nuclei of 15.2 G and a linewidth of 10.8 G.

The spin density of the styrene radical was calculated by DFT (B3LYP/def2TZVPP, smd=water), showing the contribution of carbon atoms 11 and 3, which can be interpreted as the existence of two resonant forms of the radical. The greater contribution comes from the terminal C3 (47%).

Mulliken charges and spin densities:

1 C	-0.014879	0.013012
2 H	0.175686	-0.001476
3 C	-0.083419	0.469174
4 H	0.158345	-0.013479
5 H	0.177072	-0.017156
6 C	0.116765	0.174044
7 C	-0.094031	0.083400
8 C	-0.108728	0.109248
9 C	-0.116262	-0.029664
10 C	-0.111838	-0.051204
11 C	-0.025185	0.282078
12 H	0.183269	-0.004106
13 H	0.178173	-0.003715
14 H	0.185357	0.000264
15 H	0.185111	0.000911
16 H	0.194564	-0.011329



Isotropic Fermi Contact Couplings

Atom	a.u.	MegaHertz	Gauss	10(-4) cm-1
1 C	-0.01402	-15.75697	-5.62248	-5.25596
2 H	-0.00024	-1.07194	-0.38250	-0.35756
3 C	0.02827	31.77850	11.33936	10.60017
4 H	-0.00677	-30.26888	-10.80069	-10.09661
5 H	-0.00706	-31.57763	-11.26769	-10.53317
6 C	0.00622	6.99743	2.49686	2.33409
7 C	0.00181	2.03307	0.72545	0.67816
8 C	0.00429	4.82666	1.72227	1.61000
9 C	-0.00933	-10.49351	-3.74434	-3.50026
10 C	-0.01094	-12.30154	-4.38949	-4.10335
11 C	0.01791	20.13302	7.18396	6.71565
12 H	-0.00165	-7.37583	-2.63188	-2.46031
13 H	-0.00198	-8.84533	-3.15623	-2.95048
14 H	0.00022	0.98452	0.35130	0.32840
15 H	0.00050	2.22548	0.79411	0.74234
16 H	-0.00426	-19.04792	-6.79677	-6.35370

The main contribution to the radical character of the molecule coming from the C3 carbon, the hyperfine coupling with H2, H4 and H5 was considered. It was found negligible for H2 and equal to ca. 11.0 G for H4 and H5. This value agrees with the simulation of the EPR spectrum that was obtained with a hyperfine coupling of 15.2 G for 2 coupling nuclei.

SUPPORTING INFORMATION

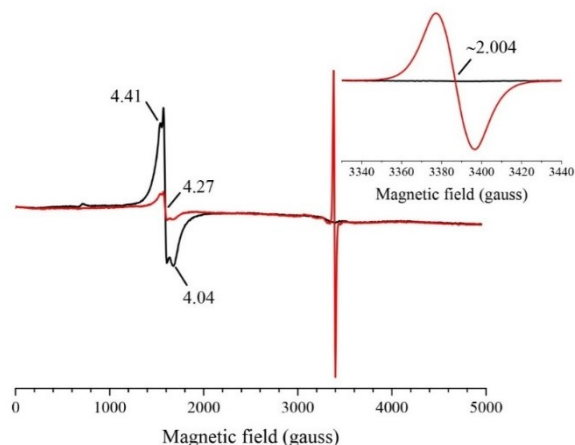


Figure S15 EPR spectra of a B&R pH 4 solution containing $[\text{Ru}^{\text{II}}(\text{bpy})_3]^{2+}$ (30 μM), MV^{2+} (20 mM), $[(\text{L}_5)\text{Fe}^{\text{II}}]^{2+}$ (100 μM) with traces of $[(\text{L}_5)\text{Fe}^{\text{III}}]^{3+}$ species and 20 mM EDTA in the dark (black) and after 30 s irradiation with 100 W m^{-2} blue LED (red). The spectra were recorded at 15 K with a modulation amplitude of 25 gauss and a microwave power of 5 mW. The microwave frequency was 9.4 GHz.

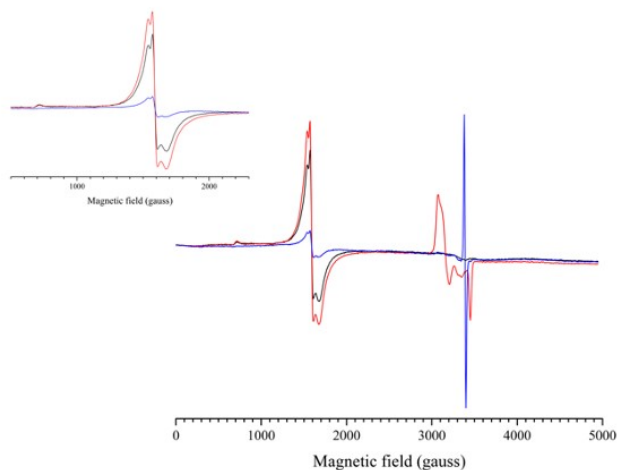


Figure S16 EPR spectral evolution of a B&R pH 4 solution containing $[\text{Ru}^{\text{II}}(\text{bpy})_3]^{2+}$ (30 μM), MV^{2+} (20 mM), $[(\text{L}_5)\text{Fe}^{\text{II}}]^{2+}$ (100 μM) with traces of $[(\text{L}_5)\text{Fe}^{\text{III}}]^{3+}$ species and 20 mM EDTA, upon irradiation. In the dark (black spectrum), after 1 s (red) and after 20 s (blue) irradiation with 100 W m^{-2} blue LED. Inset: zoom on the evolution of $[(\text{L}_5)\text{Fe}^{\text{III}}]^{3+}$ species. The spectra were recorded at 15 K with a modulation amplitude of 25 gauss and a microwave power of 5 mW. The microwave frequency was 9.4 GHz.

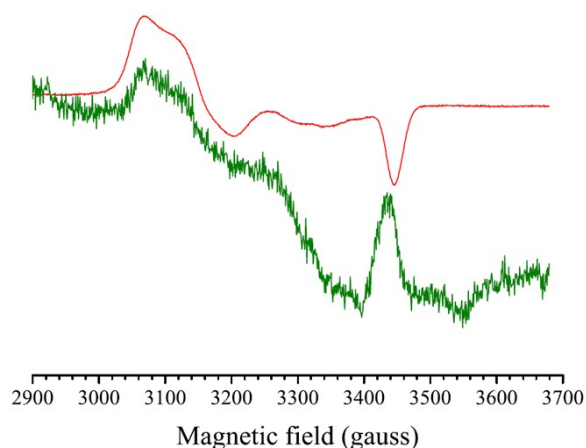
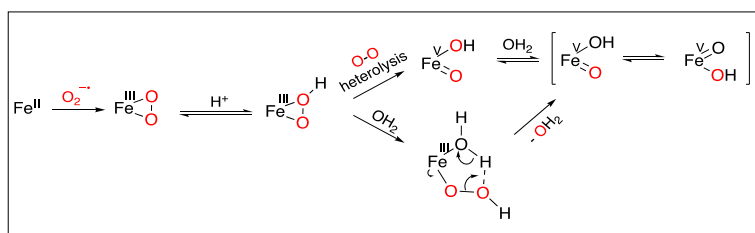


Figure S17 Amplified region of Figure 3. EPR spectra of a B&R buffer pH 4 solution containing $[\text{Ru}^{\text{II}}(\text{bpy})_3]^{2+}$ (30 μM), MV^{2+} (20 mM), $[(\text{L}_5)\text{Fe}^{\text{II}}]^{2+}$ (100 μM) and 20 mM EDTA (red) or 200 mM TEOA (green) irradiated for 1 s with 100 W m^{-2} blue LED. In red, EPR spectrum of the photo-generated low spin $[(\text{L}_5)\text{Fe}^{\text{III}}\text{-OOH}]^{2+}$ species, in green EPR spectrum of the photo-generated high spin $[(\text{L}_5)\text{Fe}^{\text{III}}\text{-}\eta^2\text{O}_2]^{2+}$ species.

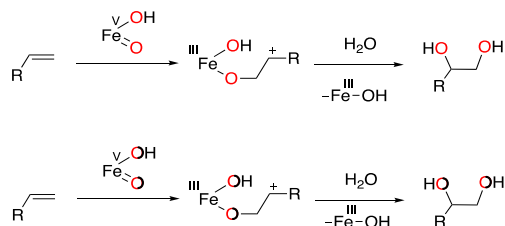
SUPPORTING INFORMATION

Cis-diol and aldehyde formation from iron hydro(peroxo) species

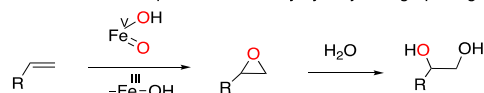


Formation of the *cis*-diol products

cis-Dihydroxylation from iron-oxo/hydroxo species

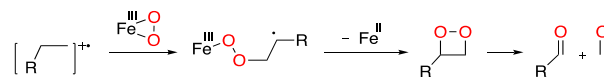


Epoxydation from iron-oxo species followed by hydrolytic ring-opening



Formation of the aldehyde derivative

Dioxetane formation from iron peroxo species followed by ring opening



Scheme S1 Proposed mechanisms for iron catalyzed sodium styrene-4-sulfonate oxidation based on literature reports. ⁷⁻¹⁰

References

- 1 C. Buron, S. Groni, N. Ségaud, S. Mazerat, D. Dragoë, C. Fave, K. Sénéchal-David, B. Schöllhorn and F. Banse, *Dalton Trans.*, 2016, **45**, 19053–19061.
- 2 A. Bohn, C. Chinaux-Chaix, K. Cheaib, R. Guillot, C. Herrero, K. Sénéchal-David, J.-N. Rebilly and F. Banse, *Dalton Trans.*, 2019, **48**, 17045–17051.
- 3 A. Bohn, K. Sénéchal-David, J.-N. Rebilly, C. Herrero, W. Leibl, E. Anxolabéhère-Mallart and F. Banse, *Chem. Eur. J.*, 2022, **n/a**, e202201600.
- 4 A. Bohn, Theses, Université Paris Saclay (COMUE), 2018.
- 5 K. A. Johnson, Z. B. Simpson and T. Blom, *Anal. Biochem.*, 2009, **387**, 20–29.
- 6 K. A. Johnson, Z. B. Simpson and T. Blom, *Anal. Biochem.*, 2009, **387**, 30–41.
- 7 W. N. Oloo and L. Que, *Acc. Chem. Res.*, 2015, **48**, 2612–2621.
- 8 I. Gamba, Z. Codolà, J. Lloret-Fillol and M. Costas, *Coord. Chem. Rev.*, 2017, **334**, 2–24.
- 9 Y. Feng, J. England and L. Que, *ACS Catal.*, 2011, **1**, 1035–1042.
- 10 W. N. Oloo, A. J. Fielding and L. Que, *J. Am. Chem. Soc.*, 2013, **135**, 6438–6441.